Energy Engineering

Tech Science Press

DOI: 10.32604/ee.2022.019284

ARTICLE

A Novel Aquila Optimizer Based PV Array Reconfiguration Scheme to Generate Maximum Energy under Partial Shading Condition

Dong An[1], Junqing Jia[1], Wenchao Cai[1], Deyu Yang[1], Chao Lv[1], Jiawei Zhu[2] and Yingying Jiao[3,*]

[1]Inner Mongolia Power Research Institute, Huhhot, 010020, China

[2]School of Information Engineering, Chang'an University, Xi'an, 710064, China

[3]School of Information and Electrical Engineering, Shandong Jianzhu University, Jinan, 250101, China

[*]Corresponding Author: Yingying Jiao. Email: yingying.jiao@outlook.com

Received: 14 September 2021 Accepted: 24 February 2022

ABSTRACT

This paper develops a real-time PV arrays maximum power harvesting scheme under partial shading condition (PSC) by reconfiguring PV arrays using Aquila optimizer (AO). AO is based on the natural behaviors of Aquila in capturing prey, which can choose the best hunting mechanism ingeniously and quickly by balancing the local exploitation and global exploration via four hunting methods of Aquila: choosing the searching area through high soar with the vertical stoop, exploring in different searching spaces through contour flight with quick glide attack, exploiting in convergence searching space through low flight with slow attack, and swooping through walk and grabbing prey. In general, PV arrays reconfiguration is a problem of discrete optimization, thus a series of discrete operations are adopted in AO to enhance its optimization performance. Simulation results based on 10 cases under PSCs show that the mismatched power loss obtained by AO is the smallest compared with genetic algorithm, particle swarm optimization, ant colony algorithm, grasshopper optimization algorithm, and butterfly optimization algorithm, which reduced by 4.34% against butterfly optimization algorithm.

KEYWORDS

PV array reconfiguration; partial shading condition; Aquila optimizer; maximum power extraction; total-cross-tied

Nomenclature

Variables

V_D	the entire output voltage of the PV array
V_{ap}	the maximum voltage of array at the pth row
I_D	the whole current flowing through each column of PV arrays
I_{pq}	output current across the pth row and the qth column of PV array
$P(C)$	the output power of the testing PV power plant at the Cth case of PSC
n	the number of sub-systems of the testing PV power plant
f	objective function
x_{pq}	the electrical connection state of PV arrays at the pth row and the qth column
X_{ij}	the ith candidate solution with dimension j

$X_{\mathrm{M}}(t)$	the mean value of current solutions at the tth iteration
$X_{\mathrm{best}}(t)$	the highest-quality solution gained during the tth iteration
Levy(D)	the levy flight distribution function
QF	the quality function used to balance the search methods
$\boldsymbol{x}_q$	the solution vector of arrays at the qth column
P_{PSC}	maximum output power of PV array under PSC
P_{max}	maximum output power of the testing PV power plant with 30 runs
P_{mean}	mean output power of the testing PV power plant with 30 runs

Parameters

UB	upper bound of search spaces
LB	lower bound of search spaces
T	maximum iteration number
V_{OC}	open-circuit voltage of PV array
I_{SC}	short-circuit voltage of PV array
P_{STC}	maximum output power of PV array under standard condition

Indices

p	index of row
q	index of column
t	index of iteration

Performance evaluation indices

FF	fill factor
ΔP_{MMPL}	mismatched power loss
$\eta(\%)$	efficiency

Abbreviations

ACO	ant colony algorithm
AO	Aquila optimizer
BOA	butterfly optimization algorithm
GA	genetic algorithm
GOA	grasshopper optimization algorithm
MPPT	maximum power point tracking
OAR	optimal PV array reconfiguration
PSC	partial shading condition
PSO	particle swarm optimization
TCT	total-cross-tied

1 Introduction

Recently, excessive energy demand has caused severe environmental deterioration and rapid energy exhaustion such as coal, oil, and natural gas, which requires a profound energy transformation due to the energy crisis [1–3]. In particular, solar energy is widely deemed as one desirable candidate, which

has been widely employed in PV power generation [4–7]. Nevertheless, fixed free-standing PV systems are easily affected by various dynamic environmental conditions, which leads to mismatch loss and power loss, uneven irradiance and temperature, together with partial shading condition (PSC) [8–10]. Among them, PSC is mainly caused by clouds, trees, buildings, dust accumulation, bird droppings, and snow [11].

To solve these thorny obstacles caused by PSC, a wide range of solutions have been proposed such as installing bypass diodes in parallel on PV panel [12] and implementing maximum power point tracking (MPPT) techniques [13]. However, the connection of bypass diodes will engender power mismatch due to multi-peak characteristics in PV panels [12]. Meanwhile, MPPT technique is troublesome to apply in large-scale PV power stations because of the complicated execution and control cost [13].

Nowadays, PV array reconfiguration has been envisaged as a highly competitive strategy to harvest maximum power output under different PSCs, which basic principle is to rearrange the shadows in the same column of PV arrays through physical relocation (PR) [14], electrical rewiring (ER) [15] and electrical array reconfiguration (EAR) [16] to equalize the effect of any concentrated PSC. PV array reconfiguration can generally be categorized into fixed and dynamic reconfigurations according to whether the electrical interconnection alters. Nowadays, plenty of static reconfiguration methods have been proposed based on PR, ER, or both, e.g., fixed reconfiguration [17], column index method [18], special connection method [19], and odd-even configuration [20]. The obvious determination of static reconstruction is that it cannot respond effectively to the dynamic changes of the shadow. On the contrary, dynamic reconfiguration can effectively cope with various shadows. Thus far, many topologies have been widely used on dynamic reconfiguration, like series-parallel, total-cross-tied (TCT) [21], Suduku, and so on.

In recent years, an optimal PV array reconfiguration (OAR) via various meta-inspiration algorithms is proposed, such as genetic algorithm (GA) [22], particle swarm optimization (PSO) [23], ant colony algorithm (ACO) [24], grasshopper optimization algorithm (GOA) [25], and butterfly optimization algorithm (BOA) [26], which can seek the optimal power output from multiple MPPs under unequal solar irradiation for TCT topology. However, these meta-inspiration algorithms tend to easily fall into the low-quality local optimum due to inherent defects of strong randomness.

Therefore, this work devises a new Aquila optimizer (AO) to extract the maximum power of PV power plants under PSC in real-time. For validation, a complete 15×15 TCT PV array reconfiguration model is implemented and tested in simulation. The main novelties of this work are outlined as follows:

- An AO based real-time maximum power harvesting strategy from PV arrays under PSC by reconfiguring PV arrays is proposed.
- Compared to the original AO [27], the proposed approach carries out a series of discrete operations to address the discrete problem of PV array reconfiguration, which considerably enhances its application feasibility in solving any discrete optimization problem.
- 10 cases under PSCs are designed to simulate possible shadows caused by clouds, trees, buildings, dust accumulation, bird droppings, and snow. Besides, the effectiveness of AO on PV array reconfiguration is tested under such 10 shadows.

The rest sections are organized as follows: Section 2 presents the mathematical model of TCT PV array reconfiguration; Section 3 introduces AO and the discrete design of AO; Section 4 provides the design of AO based OAR; Section 5 shows the results and discussion of simulation; and Section 6 gives the conclusions.

2 TCT PV Array Reconfiguration Modelling

2.1 TCT-Connected PV Arrays

TCT-connected PV arrays are connected in parallel in each row, while these rows are connected in series. Because the voltages at both ends of each row are equal, the entire output voltage of the PV array is able to be modeled as

$$V_{\mathrm{D}} = \sum_{p=1}^{F} V_{\mathrm{a}p} \tag{1}$$

where $V_{\mathrm{a}p}$ is the maximum voltage of array at the pth row.

The law of Kirchhoff current indicates that the whole current flowing through each column of PV arrays can be described as

$$I_{\mathrm{D}} = \sum_{q=1}^{F} \left(I_{pq} - I_{(p+1)q}\right) = 0, p = 1, 2, \ldots, 9, \mathrm{A}, \ldots, \mathrm{F} \tag{2}$$

where I_{pq} means output current across the pth row and the qth column of PV array.

2.2 Performance Evaluation

To evaluate the performance of OAR under PSC using AO, three indices (fill factor, mismatched power loss, and efficiency) are introduced, as follows:

Fill factor (FF): which is represented as the ratio of maximum output power under PSC (P_{PSC}) to the product of the open-circuit voltage (V_{OC}) and short circuit current (I_{SC}).

$$\mathrm{FF} = \frac{P_{\mathrm{PSC}}}{V_{\mathrm{OC}} \times I_{\mathrm{SC}}} \tag{3}$$

Mismatched Power Loss (ΔP_{MMPL}): which is described as the difference between maximum output power under the standard condition (P_{STC}) and P_{PSC}. The standard condition is defined as the solar irradiation of 1000 W/m^2 and the operation temperature of 25°C.

$$\Delta P_{\mathrm{MMPL}} = P_{\mathrm{STC}} - P_{\mathrm{PSC}} \tag{4}$$

Efficiency (η%): which is defined as the ratio of P_{PSC} to P_{STC}, it can be calculated by

$$\eta(\%) = \frac{P_{\mathrm{PSC}}}{P_{\mathrm{STC}}} \tag{5}$$

3 Aquila Optimizer

AO is designed by simulating the natural behavior of Aquila in capturing prey. Aquila's pointed hook-shaped beak and sharp claws can help them quickly catch all kinds of prey, such as hares, marmots, squirrels, and other ground animals. Most Aquila can choose the best hunting method ingeniously and quickly according to the situation.

3.1 Principle of Aquila Optimizer

3.1.1 Solutions Initialization

Initial population of AO is randomly produced within the upper bound (UB) and lower bound (LB) according to the specific questions. It can be described by

$$X_{ij} = \text{rand} \times \left(UB_j - LB_j\right), i = 1, 2, \ldots, N \quad j = 1, 2, \ldots, Dim \tag{6}$$

where X_{ij} means the ith candidate solution with dimension j; N is population number; Dim is the dimension of the specific question; rand means a random number; LB_j and UB_j denote to the jth lower bound and upper bound, respectively.

3.1.2 Mathematical Model of Aquila Optimizer

AO modeling is mainly realized by simulating Aquila's behavior when they are hunting: (1) choosing the searching area through high soar with the vertical stoop, (2) exploring in different searching spaces through contour flight with quick glide attack, (3) exploiting in convergence searching area through low flight with slow attack, and (4) swooping through the walk and grabbing prey. AO can switch between exploration and exploitation based on the condition: $t \leq \frac{2}{3} \times T$.

Step 1: Expanded exploration (X_1)

Aquila explores widely the searching area by high soar, as shown in Fig. 1a. This behavior is expressed as

$$X_1(t+1) = X_{\text{best}}(t) \times (1 - \frac{t}{T}) + (X_{\text{M}}(t) - X_{\text{best}}(t) \times \text{rand}) \tag{7}$$

where t means the current iteration and T denotes the total iterations; $X_1(t+1)$ denotes the solution at the (t+1)th iteration; $X_{\text{best}}(t)$ means the highest-quality solution gained during the tth iteration; rand randomly chooses from [0,1]; $X_{\text{M}}(t)$ represents the mean value of current solutions at the tth iteration, which is written by

$$X_{\text{M}}(t) = \frac{1}{N}\sum_{i=1}^{N} X_i(t) \tag{8}$$

Step 2: Narrowed exploration (X_2)

AO explores the area where the target prey appears to be ready for attacking, as described in Fig. 1b. This behavior is presented as

$$X_2(t+1) = X_{\text{best}}(t) \times \text{Levy}(D) + X_{\text{R}}(t) + (y - x) \times \text{rand} \tag{9}$$

where $X_2(t+1)$ indicates the solution at the (t+1)th iteration; $X_{\text{R}}(t)$ selects randomly from [1, N] at the tth iteration; D means the dimension of search space; and the function that expresses levy flight distribution is written by

$$\text{Levy}(D) = s \times \frac{u \times \sigma}{|v|^{\frac{1}{\beta}}} \tag{10}$$

where $s = 0.01$, u and v denote random numbers between 0 and 1. σ is calculated by

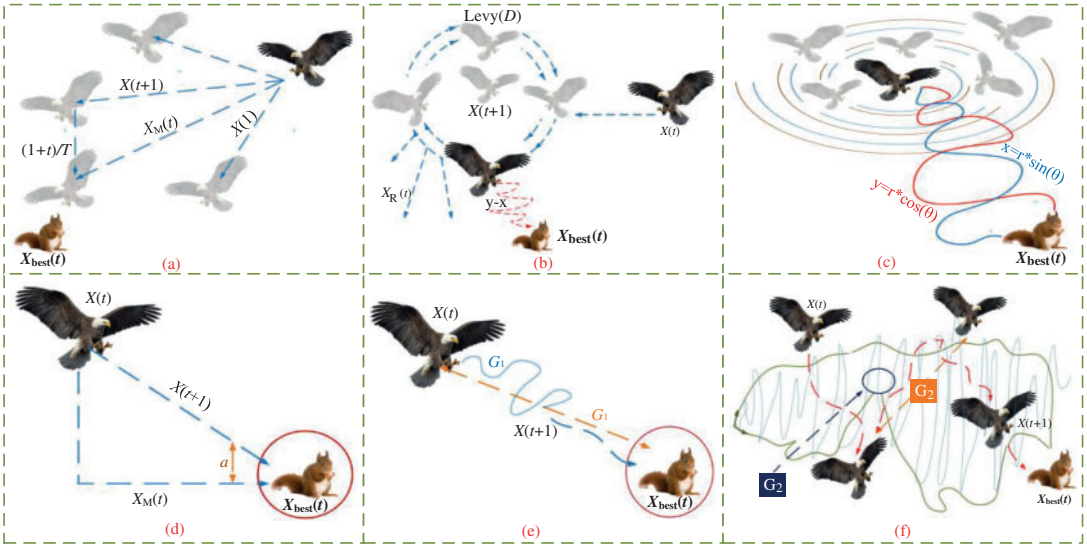

Figure 1: The behavior of the Aquila: (a) High soar with the vertical stoop; (b) Contour flight with quick glide attack; (c) Spiral shape; (d) Low flight with a slow attack; (e) Walk and grab prey; (f) The effects of the quality function (QF), G_1, and G_2 on the behavior of the AO

$$\sigma = \left(\frac{\Gamma(1+\beta) \times \sin\left(\frac{\pi\beta}{2}\right)}{\Gamma\left(\frac{1+\beta}{2}\right) \times \beta \times 2^{\left(\frac{\beta-1}{2}\right)}} \right) \tag{11}$$

where $\beta = 1.5$, x and y that expresses the spiral shape in the search are expressed as

$$y = r \times \cos(\theta) \tag{12}$$

$$x = r \times \sin(\theta) \tag{13}$$

where

$$r = r_1 + U \times D_1 \tag{14}$$

$$\theta = -\omega \times D_1 + \theta_1 \tag{15}$$

$$\theta_1 = \frac{3 \times \pi}{2} \tag{16}$$

where r_1 is a value between 1 and 20, which is used to fix the number of searching cycles; $U = 0.00565$. D_1 is integer number; and $\omega = 0.005$. The spiral behavior of AO is shown in Fig. 2c.

Step 3: Expanded exploitation (X_3)

AO exploits the range where preys appear, and then approaches and attacks it, as shown the Fig. 1d. This behavior is presented as

$$X_3(t+1) = (X_{\text{best}}(t) - X_M(t)) \times \alpha - \text{rand} + ((UB - LB) \times \text{rand} + LB) \times \delta \tag{17}$$

where $X_3(t+1)$ means the solution at the $(t+1)$th iteration; α and δ are the parameters used to adjust exploitation ($\alpha = \delta = 0.1$).

Step 4: Narrowed exploitation (X_4)

Fig. 1e describes the behavior that AO attacks the prey in the last location, which is presented as

$$X_4(t+1) = QF \times X_{\text{best}}(t) - (G_1 \times X(t) \times \text{rand}) - G_2 \times \text{Levy}(D) + \text{rand} \times G_1 \tag{18}$$

where $X_4(t+1)$ is the solution of the $(t+1)$th iteration; QF is applied to balance search methods, which is written by Eq. (19); G_1 generated by Eq. (20) denotes various motions that Aquila tracks the target in the process of exploitation; G_2 produced by Eq. (21) denotes the flight slope that Aquila tracks the target in the process of exploitation; $X(t)$ is the current solution at the tth iteration; Fig. 2f provides the influences of QF, G_1, and G_2 on the behavior of the AO.

$$QF(t) = \frac{2 \times \text{rand} - 1}{t^{(1-T)^2}} \tag{19}$$

$$G_1 = 2 \times \text{rand} - 1 \tag{20}$$

$$G_2 = 2 \times \left(1 - \frac{t}{T}\right) \tag{21}$$

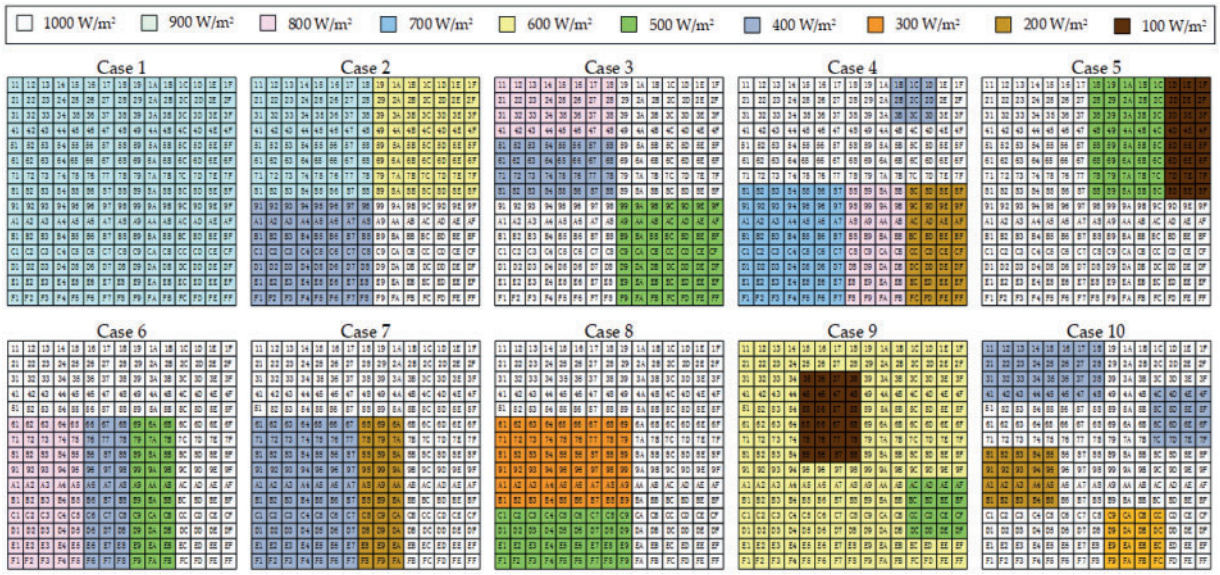

Figure 2: The irradiation distribution of the 15 × 15 PV arrays under 10 cases of PSCs

3.2 Discrete Design of Aquila Optimizer

Reconfiguring PV arrays is a problem of discrete optimization. To apply the excellent optimization performance of AO for solving this problem, a series of discrete designs are performed on AO, as follows:

3.2.1 Discretization for Initial Population

Obviously, the method of population initialization shown in Eq. (10) is not suitable for PV array reconfiguration. Hence, An $\boldsymbol{N}$ matrix is introduced to represent the initial population of OAR modeling, which can be written as

$$\boldsymbol{N} = \{[\boldsymbol{C}]_1, [\boldsymbol{C}]_2, [\boldsymbol{C}]_3, \ldots, [\boldsymbol{C}]_{n_{\text{pop}}}\} \tag{22}$$

where $\boldsymbol{C}$ is a 15 × 15 matrix created by Eq. (23) to indicate the initial electrical connection state of PV arrays. n_{pop} is the number of population.

At the process of PV array reconfiguration, each PV array only exchanges with another PV array in the same column. Thus, the optimization variables should satisfy the following constraints:

$$\begin{cases} x_{pq} \in \{1, 2, \ldots, 9, \text{A}, \ldots, \text{F}\}, p = 1, 2, \ldots, 9, \text{A}, \ldots, \text{F}; q = 1, 2, \ldots, 9, \text{A}, \ldots, \text{F} \\ \cup_{p=0}^{F} x_{pq} = \{1, 2, \ldots, 9, \text{A}, \ldots, \text{F}\}, q = 1, 2, \ldots, 9, \text{A}, \ldots, \text{F} \end{cases} \tag{23}$$

where x_{pq} denotes the electrical connection state of PV arrays at the pth row and the qth column. To satisfy the constraints in Eq. (22), a Matlab function 'randperm (n)' is introduced, as follows:

$$\begin{cases} \boldsymbol{C}_q = \text{randperm}\,(15), q = 1, 2, \ldots, 9, \text{A}, \ldots, \text{F} \\ \boldsymbol{C} = \left[\boldsymbol{C}_1, \boldsymbol{C}_2, \ldots, \boldsymbol{C}_q, \ldots, \boldsymbol{C}_9, \boldsymbol{C}_{\text{A}}, \ldots, \boldsymbol{C}_{\text{F}}\right] \end{cases} \tag{24}$$

where 'randperm (15)' means to randomly sort 15 data in a column; $\boldsymbol{C}_q$ represents the qth column of the $\boldsymbol{C}$.

3.2.2 Discretization for Optimization Process

AO switches between exploration and exploitation according to the situation to choose the best hunting method ingeniously and quickly. To make the optimization method suitable for PV array reconfiguration, the sequence of solutions optimized by Eqs. (7)–(21) will be chosen to reassign the electrical connection state of each column of PV arrays, as follows:

$$s_{pq} = \text{rank}(x_{pq}, \boldsymbol{x}_q) \tag{25}$$

where $\boldsymbol{x}_q = [X_1, X_2, \ldots, X_i, \ldots, X_9, X_{\text{A}}, \ldots, X_{\text{F}}]$ is the solution vector of arrays at the qth column; rank $\left(x_{pq}, \boldsymbol{x}_q\right)$ denotes the order of x_{pq} among all solutions $\boldsymbol{x}_q$, which is designed in ascending order.

4 Design of Aquila Optimizer Based OAR

Since the physical position of all arrays in TCT configuration is fixed, an OAR model via electrical switches is introduced to reconfigure the position of arrays. Firstly, a discrete design for AO is performed for OAR model to obtain the optimal electrical connection state. After that, the physical position of PV arrays is rearranged via electrical switches in conformity with the obtained electrical connection state.

4.1 Objective Function

The primary goal of PV power plant is to extract the maximum output power under PSC, and its objective function is expressed as

$$f = \max P(C) = \max\left(n \times I_{\text{D}}(C) \times V_{\text{D}}(C)\right) \tag{26}$$

where P(C) is the output power of the testing PV power plant at the Cth case of PSC; n is the number of sub-systems of the testing PV power plant.

4.2 Execution Procedure

On the whole, the entire executive procedure of OAR based on AO is provided in Table 1.

Table 1: Executive procedure of OAR based on AO

Input the real-time predictive weather conditions;
Initialize the parameters and population by Eqs. (22)–(24) of OAR based on AO;
Set $t = 1$;
Calculate the objective function $f(X(t))$ of all the searching individuals by Eqs. (1) and (2) and Eq. (26);
For $t = 2$: T
Update the mean value of the current solution $X_M(t)$;
Update the x, y,G_1,G_2, Levy(D), etc.;
If $t \leqslant (2/3) * T$ then
If rand $\leqslant 0.5$ then
Update the current solution X_1 using Eqs. (7) and (25);
If $f(X_1(t+1)) < f(X(t))$ then
$X(t) = (X_1(t+1))$
If $f(X_1(t+1)) < f(X_{best}(t))$ then
$X_{best}(t) = X_1(t+1)$
End If
End If
Else:
Update the current solution X_2 using Eqs. (9) and (25);
If $f(X_2(t+1)) < f(X(t))$ then
$X(t) = (X_2(t+1))$
If $f(X_2(t+1)) < f(X_{best}(t))$ then
$X_{best}(t) = X_2(t+1)$
End If
End If
End If
Else:
If rand < 0.5 then
Update the current solution X_3 using Eqs. (17) and (25);
If $f(X_3(t+1)) < f(X(t))$ then
$X(t) = (X_3(t+1))$
If $f(X_3(t+1)) < f(X_{best}(t))$ then
$X_{best}(t) = X_3(t+1)$
End If
End If
Else:
Update the current solution X_4 using Eqs. (18) and (25);
If $f(X_4(t+1)) < f(X(t))$ then
$X(t) = (X_4(t+1))$
If $f(X_4(t+1)) < f(X_{best}(t))$ then

(Continued)

Table 1 (continued)

1: Input the real-time predictive weather conditions;

40: $X_{best}(t) = X_4(t+1)$
41: **End If**
42: **End If**
43: **End If**
44: **End If**
45: **End For**
46: Output the electrical connection state of OAR X_{best};
47: Re-execute AO from step 1 to step 46 at the next case of shadow.

5 Case Studies

5.1 Operating Conditions Setting

In this work, AO is applied to a test PV power station under 10 cases of PSCs (see Fig. 2) to validate its application reliability. PV power station is composed of 20 identical subsystems while each subsystem is formed by 15 × 15 TCT arrays. Note that the 10 cases of PSCs are based on the simulation of shading effects caused by clouds, trees, buildings, dust accumulation, bird droppings, and snow, in which different color blocks represent different irradiation intensity, i.e., white block is 1000 W/m^2, pale-yellow block is 900 W/m^2, light blue block is 800 W/m^2 and others shown in Fig. 2. Table 2 gives the electrical characteristics of each PV array. Moreover, five algorithms (e.g., GA [22], PSO [23], ACO [24], GOA [25], and BOA [26]) are used for performance comparison with that of AO. T and N of all algorithms are unified to be 200 and 50, respectively to guarantee a fair and reliable comparison. Because the proposed method is based on meta-heuristic algorithm, each run will inevitably produce different results. To avoid this drawback to the greatest extent and obtain the global optimal solution, 30 runs of AO are undertaken on Matlab/Simulink 2017b using a personal computer with an Intel(R) Core (TM) i5-8400 CPU @ 2.80 GHz and 12 GB RAM. The applied solver is ode23 with the variable-step size of 10^{-3} s.

Table 2: Electrical characteristics of each PV array

Parameter	Value
Number of strings in parallel	10
Number of modules in series each string	5
Number of cells each module	60
Maximum output power each module	224.98 W
Open circuit voltage each module	36.24 V
Short-circuit current each module	8.04 A
Voltage of maximum power point each module	30.24 V
Current of maximum power point each module	7.44 A

5.2 Result Analysis

Table 3 provides the optimization results of OAR under 10 cases of PSCs in 30 runs of six algorithms. Here, P_{max} and P_{mean} are the maximum and mean values of output power in 30 independent runs. From Table 3, it can be seen that AO acquires the optimal P_{max} and P_{mean} (in bold). In addition, three evaluation indices (FF, ΔP_{MMPL} and η) are introduced to further validate the performance of AO. The calculation of the three indicators depends on the total P_{mean} of 10 cases of PSCs. One can see clearly that AO can get the largest FF and η as well as the smallest ΔP_{MMPL} compared with other five algorithms. Particularly, FF and η obtained by AO are 1.67% and 1.68% higher than those of BOA, respectively, while ΔP_{MMPL} has a 4.34% decrease.

Table 3: Optimization results of OAR under 10 cases of PSCs in 30 runs of six algorithms

Case	GA		PSO		ACO		GOA		BOA		AO	
	P_{max} (MW)	P_{mean} (MW)	P_{max} (MW)	P_{mean} (MW)	P_{max} (MW)	P_{mean} (MW)	P_{max} (MW)	P_{mean} (MW)	P_{max} (MW)	P_{mean} (MW)	P_{max} (MW)	P_{mean} (MW)
1	45.56	45.56	45.56	45.56	45.56	45.56	45.56	45.56	45.56	45.56	**45.56**	**45.56**
2	35.10	34.65	35.43	34.92	35.44	35.00	35.43	34.82	35.10	34.63	**35.77**	**35.03**
3	38.13	37.21	38.13	37.67	38.13	37.59	37.80	37.65	38.13	37.19	**38.47**	**37.73**
4	37.12	36.68	37.12	36.40	37.12	36.78	36.78	36.41	37.12	36.38	**37.12**	**36.82**
5	39.48	38.53	39.48	39.45	39.48	39.48	39.82	39.42	39.48	38.51	**39.82**	**39.48**
6	39.82	39.41	39.82	39.50	40.16	39.61	39.82	39.47	39.82	39.39	**40.16**	**39.72**
7	34.42	32.88	34.42	33.23	34.42	33.88	34.42	33.34	34.42	32.85	**35.10**	**34.00**
8	36.78	35.70	36.78	36.22	36.78	36.30	37.12	36.26	36.78	35.65	**37.12**	**36.30**
9	26.66	25.62	26.66	26.38	26.66	26.54	26.66	26.38	26.66	25.57	**26.66**	**26.57**
10	36.45	35.33	36.45	35.75	36.79	35.84	36.45	35.84	36.45	35.31	**36.79**	**35.87**
FF (Total)	0.5515		0.5569		0.5592		0.5570		0.5507		0.5599	
MMloss (Total) (MW)	144.635		141.125		139.625		141.055		145.165		139.125	
η%	71.43		72.12		72.42		72.13		71.32		72.52	

The optimal solution of the 15 × 15 PV arrays reconfigured by AO is provided in Fig. 3, where concentrated shadows of all PV arrays in Fig. 2 are re-distributed to different rows. It dramatically increases the output power of PV plants. Neglecting the voltage drop of bypass diode, the maximum output power obtained by AO under the 4th case of PSC is 28.08% higher than that without optimization, as described in Fig. 4. Furthermore, the number of power peaks in the *P-V* curve can be significantly reduced by using AO. Fig. 5 gives the convergence result of the AO algorithm for 15 x 15 PV arrays at the 4th case of PSC. It can be seen that AO can quickly converge to a high-quality optimal solution.

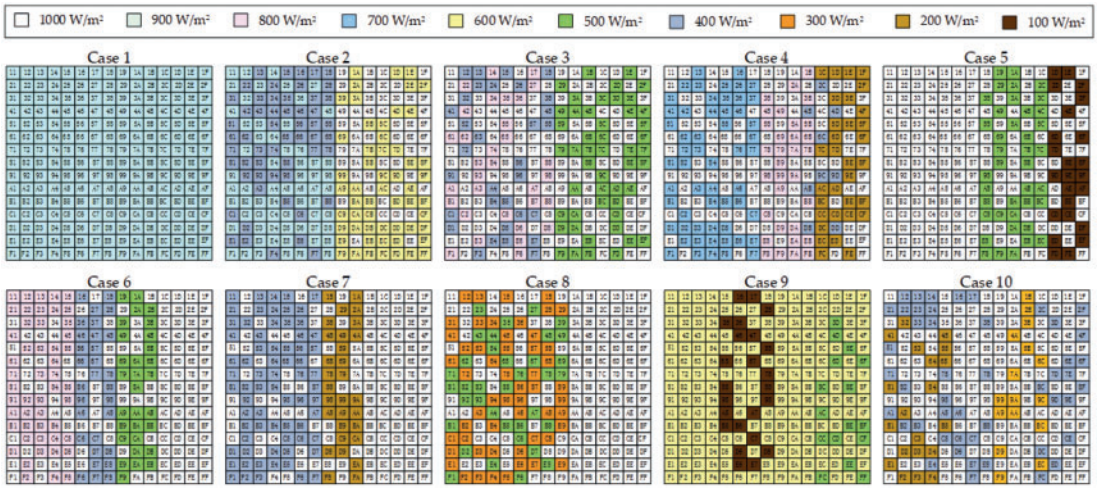

Figure 3: Optimal solution of the 15 × 15 PV arrays reconfigured by AO with 10 cases of PSCs

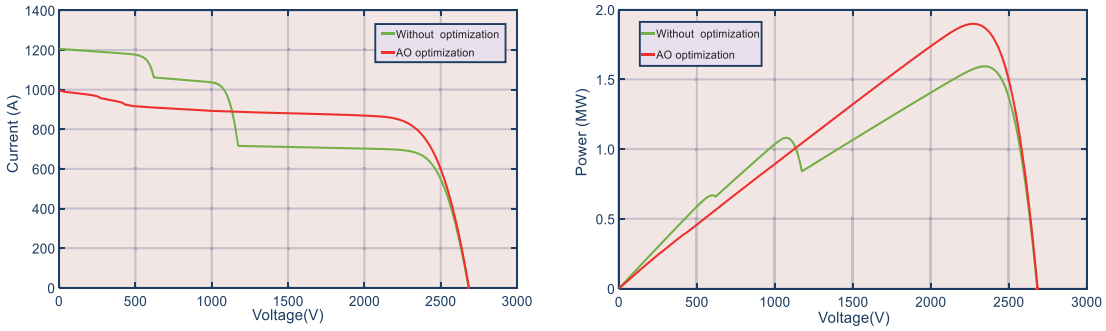

(a) (b)

Figure 4: Comparison result of the sub-system acquired by without optimization and AO at the 4th case of PSC. (a) *I-V* curves, and (b) *P-V* curves

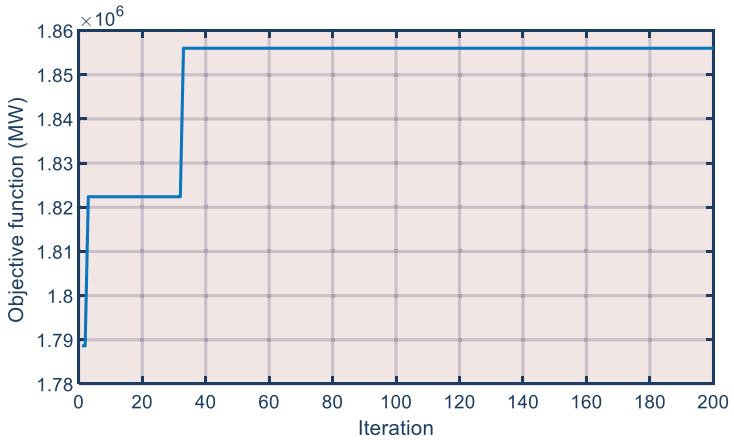

Figure 5: The convergence diagram of the AO for 15 × 15 PV arrays at the 4th case of PSC

6 Conclusions

An AO based OAR is proposed for real-time maximum power extraction under PSC of PV arrays in this work, which contributions are drawn as follows:

(1) AO contains a series of discrete operations during optimization to solve the discrete problem of PV array reconfiguration, which owns great potential to apply in other complex discrete optimization problems.

(2) This work comprehensively considers the impact of PSC caused by clouds, trees, buildings, dust accumulation, bird droppings, and snow for PV array and simulates the 10 cases of PSCs based on this impact to validate the application reliability of AO under various PSCs.

(3) A series of experiments based on 10 cases of PSCs are designed to validate the optimization performance of AO compared against five well-known algorithms (e.g., GA, PSO, ACO, GOA, and BOA). Simulation results indicate that the mismatched power loss obtained by AO is the smallest, which can be decreased by 4.34% against BOA. Furthermore, it can be seen that the number of multiple peaks caused by the various PSCs can be significantly reduced by AO.

Future studies will focus on the following aspects:

(1) Apply the proposed AO based OAR to larger-scale PV arrays.

(2) Apply discrete AO to solve other discrete optimization problems.

Funding Statement: This work is supported by the Scientific Research Projects of Inner Mongolia Power (Group) Co., Ltd. (Internal Electric Technology (2021) No. 3).

Conflicts of Interest: Authors Deyu Yang, Junqing Jia, Wenli Wu, Wenchao Cai, Dong An are employed by Inner Mongolia Power Research Institute. The remaining authors declare that the research was conducted in the absence of any commercial or financial relationships that could be construed as a potential conflict of interest.

References

1. Murty, V. V. S. N., Kumar, A. (2020). Multi-objective energy management in microgrids with hybrid energy sources and battery energy storage systems. *Protection and Control of Modern Power Systems, 5(1),* 1–20. DOI 10.1186/s41601-019-0147-z.
2. Yang, B., Yu, T., Shu, H. C., Dong, J., Jiang, L. (2018). Robust sliding-mode control of wind energy conversion systems for optimal power extraction via nonlinear perturbation observers. *Applied Energy, 210(1),* 711–723. DOI 10.1016/j.apenergy.2017.08.027.
3. Yang, B., Wang, J. B., Zhang, X. S., Yu, T., Yao, W. et al. (2020). Comprehensive overview of meta-heuristic algorithm applications on PV cell parameter identification. *Energy Conversion and Management, 208(5),* 112595. DOI 10.1016/j.enconman.2020.112595.
4. Bozorg, M., Bracale, A., Caramia, P., Carpinelli, G., Falco, P. D. (2020). Bayesian bootstrap quantile regression for probabilistic photovoltaic power forecasting. *Protection and Control of Modern Power Systems, 5(3),* 218–229. DOI 10.1186/s41601-020-00167-7.
5. Kumar, D. S., Savier, J. S., Biju, S. S. (2020). Micro-synchrophasor based special protection scheme for distribution system automation in a smart city. *Protection and Control of Modern Power Systems, 5(1),* 97–110. DOI 10.1186/s41601-020-0153-1.
6. Erdiwansya, E., Mahidin, M., Husin, H., Nasaruddin, N., Zaki, M. et al. (2021). A critical review of the integration of renewable energy sources with various technologies. *Protection and Control of Modern Power Systems, 6(1),* 37–54. DOI 10.1186/s41601-021-00181-3.

7. Shang, L. Q., Guo, H. C., Zhu, W. W. (2020). An improved MPPT control strategy based on incremental conductance algorithm. *Protection and Control of Modern Power Systems, 5(2),* 176–184. DOI 10.1186/s41601-020-00161-z.
8. Yang, B., Yu, T., Zhang, X. S., Li, H. F., Shu, H. C. et al. (2019). Dynamic leader based collective intelligence for maximum power point tracking of PV systems affected by partial shading condition. *Energy Conversion and Management, 179(18),* 286–303. DOI 10.1016/j.enconman.2018.10.074.
9. Xi, L., Wu, J., Xu, Y., Sun, H. (2020). Automatic generation control based on multiple neural networks with actor-critic strategy. *IEEE Transactions on Neural Networks and Learning Systems, 32(6),* 2483–2493. DOI 10.1109/TNNLS.2020.3006080.
10. Zhang, K., Zhou, B., Or, S. W., Li, C. B., Chung, C. Y. et al. (2021). Optimal coordinated control of multi-renewable-to-hydrogen production system for hydrogen fueling stations. *IEEE Transactions on Industry Applications, 10,* 3093841. DOI 10.1109/TIA.2021.3093841.
11. Fathy, A., Rezk, H., Yousri, D. (2020). A robust global MPPT to mitigate partial shading of triple-junction solar cell-based system using manta ray foraging optimization algorithm. *Solar Energy, 207(10),* 305–316. DOI 10.1016/j.solener.2020.06.108.
12. Yang, B., Zhong, L. E., Zhang, X. S., Shu, H. C., Yu, T. et al. (2019). Novel bio-inspired memetic salp swarm algorithm and application to MPPT for PV systems considering partial shading condition. *Journal of Cleaner Production, 215(3),* 1203–1222. DOI 10.1016/j.jclepro.2019.01.150.
13. Yang, B., Zhu, T. J., Wang, J. B., Shu, H. C., Sun, L. M. (2020). Comprehensive overview of maximum power point tracking algorithms of PV systems under partial shading condition. *Journal of Cleaner Production, 268(5),* 121983. DOI 10.1016/j.jclepro.2020.121983.
14. Dhanalakshmi, B., Rajasekar, N. (2018). A novel competence square based PV array reconfiguration technique for solar PV maximum power extraction. *Energy Conversion and Management, 174(2),* 897–912. DOI 10.1016/j.enconman.2018.08.077.
15. Babu, T. S., Ram, J. P., Dragičević, T., Miyatake, M., Blaabjerg, F. et al. (2018). Particle swarm optimization based solar PV array reconfiguration of the maximum power extraction under partial shading conditions. *IEEE Transactions on Sustainable Energy, 9(1),* 74–85. DOI 10.1109/TSTE.2017.2714905.
16. Rao, P. S., Ilango, G. S., Nagamani, C. (2014). Maximum power from PV arrays using a fixed configuration under different shading conditions. *IEEE Journal of Photovoltaics, 4(2),* 679–686. DOI 10.1109/JPHOTOV.2014.2300239.
17. Satpathy, P. R., Sharma, R. (2019). Power and mismatch losses mitigation by a fixed electrical reconfiguration technique for partially shaded PV arrays. *Energy Conversion and Management, 192(1),* 52–70. DOI 10.1016/j.enconman.2019.04.039.
18. Pillai, D. S., Ram, J. P., Nihanth, M. S. S., Rajasekar, N. (2018). A simple, sensorless and fixed reconfiguration scheme for maximum power enhancement in PV systems. *Energy Conversion and Management, 172(2),* 402–417. DOI 10.1016/j.enconman.2018.07.016.
19. Pareek, S., Dahiya, R. (2016). Enhanced power generation of partial shaded PV fields by forecasting the interconnection of modules. *Energy, 95(1),* 561–572. DOI 10.1016/j.energy.2015.12.036.
20. Yadav, K., Kumar, B., Swaroop, D. (2020). Mitigation of mismatch power losses of PV array under partial shading condition using novel odd even configuration. *Energy Reports, 6(1),* 427–437. DOI 10.1016/j.egyr.2020.01.012.
21. Varma, G. H. K., Barry, V. R., Jain, R. K. (2022). A total-cross-tied-based dynamic photovoltaic array reconfiguration for water pumping system. *IEEE Access, 10,* 4832–4843. DOI 10.1109/ACCESS.2022.3141421.
22. Rajan, N. A., Shrikant, K. D., Dhanalakshmi, B., Rajasekar, N. (2017). Solar PV array reconfiguration sing the concept of standard deviation and genetic algorithm. *Energy Procedia, 117,* 1062–1069. DOI 10.1016/j.egypro.2017.05.229.

23. Chen, P. Y., Chao, K. H., Liao, B. J. (2018). Joint operation between a PSO-based global MPP tracker and a PV module array configuration strategy under shaded or malfunctioning conditions. *Energies, 11(8),* 1–16. DOI 10.3390/en11082005.
24. Cao, R., Ding, Y. F., Fang, X. L., Liang, S. M., Qi, F. Y. et al. (2020). PV array reconfiguration under partial shading conditions based on ant colony optimization. *Chinese Control and Decision Conference (CCDC), 22–24,* 703–708. DOI 10.1109/CCDC49329.2020.9164084.
25. Hasanien, H. M., Al-Durra, A., Muyeen, S. M. (2016). Gravitational search algorithm-based PV array reconfiguration for partial shading losses reduction. *5th IET International Conference on Renewable Power Generation (RPG)*, pp. 21–23. London, UK.
26. Fathy, A. (2020). Butterfly optimization algorithm based methodology for enhancing the shaded PV array extracted power via reconfiguration process. *Energy Conversion and Management, 220(1),* 113115. DOI 10.1016/j.enconman.2020.113115.
27. Abualigah, L., Yousri, D., Elaziz, M. A., Ewees, A. A., Al-qaness, M. A. A. et al. (2021). Aquila optimizer: A novel meta-heuristic optimization algorithm. *Computers & Industrial Engineering, 157(11),* 107250. DOI 10.1016/j.cie.2021.107250.